
On the Evaluation of Conditional GANs

Terrance DeVries*
University of Guelph
Vector Institute
terrance@uoguelph.ca

Adriana Romero
Facebook AI Research
adrianars@fb.com

Luis Pineda
Facebook AI Research
lep@fb.com

Graham W. Taylor
University of Guelph
Vector Institute
Canada CIFAR AI Chair
gwtaylor@uoguelph.ca

Michal Drozdal
Facebook AI Research
mdrozdal@fb.com

Abstract

Conditional Generative Adversarial Networks (cGANs) are finding increasingly widespread use in many application domains. Despite outstanding progress, quantitative evaluation of such models often involves multiple distinct metrics to assess different desirable properties such as image quality, intra-conditioning diversity, and conditional consistency, making model benchmarking challenging. In this paper, we propose the Fréchet Joint Distance (FJD), which implicitly captures the above mentioned properties in a *single metric*. FJD is defined as the Fréchet Distance of the *joint distribution* of images and conditionings, making it less sensitive to the often limited per-conditioning sample size. As a result, it scales more gracefully to stronger forms of conditioning such as pixel-wise or multi-modal conditioning. We evaluate FJD on a modified version of the dSprite dataset as well as on the large scale COCO-Stuff dataset, and consistently highlight its benefits when compared to currently established metrics. Moreover, we use the newly introduced metric to compare existing cGAN-based models, with varying conditioning strengths, and show that FJD can be used as a promising *single* metric for model benchmarking.

1 Introduction

Generative models are finding progressive widespread use in many domains [6, 19, 46, 35, 44]. Among the most promising approaches, Variational Auto-Encoders (VAEs) [20], auto-regressive models [43, 42] and Generative Adversarial Networks (GANs) [9] have been driving significant progress, with the latter at the forefront of a wide-range of applications [24, 52, 32, 46, 1, 38, 34]. In particular, significant research has emerged from practical applications, which require the generation to be conditioned on prior information. For example, tasks such as image inpainting, super-resolution or text-to-image synthesis have been successfully addressed within the framework of *conditional* generation, with conditional GANs (cGANs) among the most competitive approaches. Despite these outstanding advances, quantitative evaluation of GANs remains a challenge [41, 5].

In the last few years, a significant number of evaluation metrics for GANs have been introduced in the literature [30, 50, 16, 12, 2, 33, 11, 55, 49, 37, 18]. Although there is no clear consensus on which quantitative metric is most appropriate to benchmark GAN-based models, the Inception Score (IS) [33] and Fréchet Inception Distance (FID) [12] have been extensively used. However, both IS and

*Work done during internship with Facebook AI Research.

FID were introduced in the context of *unconditional* generation and, hence, focus on capturing certain desirable properties such as *visual quality* and *sample diversity*, which do not fully encapsulate all the different phenomena that arise during conditional image generation.

In particular, in *conditional* generation, we care about *visual quality*, *intra-conditioning diversity* – i.e. sample diversity per conditioning, and *conditional consistency* – i.e. verifying that the generation respects its conditioning. Although visual quality is captured by both metrics, IS is agnostic to intra-conditioning diversity and FID only captures it indirectly.² Moreover, neither of them is able to capture conditional consistency. In order to overcome this shortcoming, researchers have resorted to reporting conditional consistency metrics in conjunction with FID [54, 29]. Consistency metrics often use some form of concept detector to ensure that the requested conditioning appears in the generated image as expected. Although intuitive to use, these metrics require pre-trained models that cover the same target concepts in the same format as the conditioning (i.e. classifiers for image-level class conditioning, object detectors for bounding box conditioning, semantic segmentation for mask conditioning), which may or may not be available off-the-shelf. Moreover, using different metrics to evaluate different desirable properties may hinder the process of model selection, as there might not be a single model that surpasses the rest in all measures. Alternatively, researchers have proposed to calculate FID per conditioning [26], which should in principle capture all desirable properties. However, it is worth noting that FID is strongly affected by the number of samples [4] and in conditional generation, *only a few samples* are usually available per conditioning (e.g. in the case of mask conditioning, we only have a single sample per unique conditioning).

In this paper we introduce a new metric called Fréchet Joint Distance (FJD), which is able to implicitly assess image quality, intra-conditioning diversity, and conditional consistency, while scaling gracefully to scenarios where each unique conditioning has a limited number of samples. FJD computes the Fréchet Distance (FD) on an embedding of the joint image-conditioning distribution and, thus, inherently has access to a larger sample size, while introducing only small computational overhead over FID. We evaluate the properties of FJD on a variant of the synthetic dSprite dataset [23] as well as the large scale COCO-Stuff dataset [7]. We provide an analysis on the behavior of both FID and FJD under different types of conditioning and evaluate existing cGAN models with the newly introduced metric. Our experiments show that (1) FJD captures the three highlighted properties of conditional generation; (2) it can be applied to any kind of conditioning (e.g. class, bounding box or mask conditioning); and (3) when applied to existing cGAN-based models, FJD demonstrates its potential to be used as a promising *unified* metric for cGAN benchmarking.

2 Related Work

Conditional GANs have witnessed outstanding progress in recent years. Significant effort has been devoted to improving training strategies and enhancing architecture designs. Training stability has been improved through the introduction of techniques such as spectral normalization [25] and the two time-scale update rule [12]. Architecturally, conditional generation has been improved through the use of auxiliary classifiers [27] and the introduction of a projection-based conditioning for the discriminator [26]. Image quality has also benefited from the incorporation of self-attention [52], as well as increases in model capacity and batch size [6].

All of this progress has led to impressive results, paving the road towards the challenging generation of more complex scenes. To this end, new forms of conditioning have been explored in the literature. A flurry of works have tackled the problem of image-to-image translation, either from a deterministic perspective [16, 57, 47], or from that of conditional generation [58, 1, 15, 22, 29], to account for the multimodal nature of the problem. Image-to-image conditional generation has also been framed as a mask-to-image or bounding box-to-image task [14, 13, 29, 54]. The vast majority of these methods are compared in terms of *qualitative assessment* (e.g. user preference studies), *visual quality* metrics such as IS or FID as well as *conditional consistency* metrics such as objection detection/segmentation mean Intersection over Union (mIoU), per pixel-accuracy or, in the case of style transfer applications, image similarity metrics such as Mean Squared Error (MSE) or Structural Similarity (SSIM). Additionally, diversity of the models is often evaluated by way of the

²FID compares image distributions and, as such, should be able to roughly capture the intra-conditioning diversity. Since it cares about image marginal distribution exclusively, it would fail to capture intra-conditioning diversity when changes only affect the image-conditioning joint distribution. See supplementary material.

Learned Perceptual Image Patch Similarity (LPIPS) [53]. Text-conditioned image generation has also been enjoying increasing attention [32, 51, 52, 40, 14, 17]. These methods follow image-to-image evaluation in the use of IS and FID to estimate visual quality, and also apply pre-trained image captioning models paired with text-based metrics such as BLEU [28], METEOR [3] or CIDEr [45] to measure conditional consistency. More recently, dialogue-conditioned image generation has also been introduced [8, 36]. In these cases, metrics evaluating object location and relational similarity are included to assess conditional consistency.

One major limitation of commonly used conditional consistency and diversity metrics is that they require having access to pre-trained models for each given task (e.g. a classification model to test class consistency). As an alternative, Intra-FID [26] has been proposed in the context of class-conditioned image generation. Intra-FID calculates an FID score separately for each conditioning and reports the average score over all conditionings. This method captures intra-class variability without requiring a dedicated pre-trained model for the dataset. However, it scales poorly with the number of unique conditions, as the computationally intensive FID calculation must be repeated for each case, and because FID behaves poorly when the sample size is small [4]. Furthermore, in cases where the conditioning cannot be broken down into a set of discrete classes (e.g. pixel-based conditioning), Intra-FID is intractable. As a result, it has not been applied beyond class-conditioning.

Beyond IS and FID, a number of GAN evaluation metrics have emerged in the literature. Most of these metrics either focus on the separability between generated images and real images [21, 30, 50, 16], compute the distance between distributions [10, 12, 2], assess sample quality and diversity from conditional or marginal distributions [33, 11, 55], measure the similarity between generated and real images [49, 48, 37, 18] or are log-likelihood based [41]. Despite this progress, there is still no clear consensus on which metrics are most appropriate to use, and the vast majority of available metrics are only concerned with unconditional generation. We refer the reader to [5] for a detailed overview and insightful discussion of existing metrics.

3 Review of Fréchet Inception Distance (FID)

FID aims to compare the statistics of generated samples to samples from a real dataset. Given two multivariate Gaussian distributions $\mathcal{N}(\boldsymbol{\mu}, \boldsymbol{\Sigma})$ and $\mathcal{N}(\hat{\boldsymbol{\mu}}, \hat{\boldsymbol{\Sigma}})$, Fréchet Distance (FD) is defined as:

$$d^2 \left((\boldsymbol{\mu}, \boldsymbol{\Sigma}), (\hat{\boldsymbol{\mu}}, \hat{\boldsymbol{\Sigma}}) \right) = \|\boldsymbol{\mu} - \hat{\boldsymbol{\mu}}\|_2^2 + \text{Tr} \left(\boldsymbol{\Sigma} + \hat{\boldsymbol{\Sigma}} - 2(\boldsymbol{\Sigma}\hat{\boldsymbol{\Sigma}})^{1/2} \right). \quad (1)$$

When evaluating a generative model, $\mathcal{N}(\boldsymbol{\mu}, \boldsymbol{\Sigma})$ represents the data (reference) distribution, obtained by fitting a Gaussian to images from a reference dataset and $\mathcal{N}(\hat{\boldsymbol{\mu}}, \hat{\boldsymbol{\Sigma}})$ represents the learned (generated) distribution, a result of fitting to samples from a generative model.

In FID, both the real images and model samples are embedded in a learned feature space using a pre-trained Inception v3 model [39]. Thus, the Gaussian distributions are defined in the embedded space. More precisely, given a dataset of images $\{\mathbf{x}^{(i)}\}_{i=0}^N$, a set of model samples $\{\hat{\mathbf{x}}^{(i)}\}_{i=0}^M$ and an Inception embedding function f , we estimate the Gaussian parameters $\boldsymbol{\mu}$, $\boldsymbol{\Sigma}$, $\hat{\boldsymbol{\mu}}$ and $\hat{\boldsymbol{\Sigma}}$ as:

$$\boldsymbol{\mu} = \frac{1}{N} \sum_{i=0}^N f(\mathbf{x}^{(i)}), \quad \boldsymbol{\Sigma} = \frac{1}{N-1} \sum_{i=0}^N \left(f(\mathbf{x}^{(i)}) - \boldsymbol{\mu} \right) \left(f(\mathbf{x}^{(i)}) - \boldsymbol{\mu} \right)^T, \quad (2)$$

$$\hat{\boldsymbol{\mu}} = \frac{1}{M} \sum_{i=0}^M f(\hat{\mathbf{x}}^{(i)}), \quad \hat{\boldsymbol{\Sigma}} = \frac{1}{M-1} \sum_{i=0}^M \left(f(\hat{\mathbf{x}}^{(i)}) - \hat{\boldsymbol{\mu}} \right) \left(f(\hat{\mathbf{x}}^{(i)}) - \hat{\boldsymbol{\mu}} \right)^T. \quad (3)$$

4 Fréchet Joint Distance (FJD)

In conditional image generation, a dataset is composed of image-conditioning pairs $\{(\mathbf{x}^{(i)}, \mathbf{y}^{(i)})\}_{i=0}^N$, where the conditioning can take variable forms, such as image-level classes, bounding box annotations or segmentation masks. The goal of conditional image generation is to produce realistic looking, diverse images $\hat{\mathbf{x}}$ that are *consistent* with the conditioning $\hat{\mathbf{y}}$. Thus, a set of model samples with corresponding conditioning can be defined as: $\{(\hat{\mathbf{x}}^{(i)}, \hat{\mathbf{y}}^{(i)})\}_{i=0}^M$.

As discussed in Section 3, the Fréchet distance compares any two Gaussians defined over arbitrary spaces. In FJD, we propose to compute the FD between two Gaussians defined over the *joint image-conditioning embedding space*. More precisely, given an image Inception embedding function f , a conditioning embedding function h and a merging function g that combines the image embedding with the conditioning embedding into a joint one, we can estimate the respective Gaussian parameters $\boldsymbol{\mu}$, $\boldsymbol{\Sigma}$, $\hat{\boldsymbol{\mu}}$ and $\hat{\boldsymbol{\Sigma}}$ as:

$$\boldsymbol{\mu} = \frac{1}{N} \sum_{i=0}^N g \left(f(\mathbf{x}^{(i)}), h(\mathbf{y}^{(i)}) \right), \quad \hat{\boldsymbol{\mu}} = \frac{1}{M} \sum_{i=0}^M g \left(f(\hat{\mathbf{x}}^{(i)}), h(\hat{\mathbf{y}}^{(i)}) \right), \quad (4)$$

$$\boldsymbol{\Sigma} = \frac{1}{N-1} \sum_{i=0}^N \left(g \left(f(\mathbf{x}^{(i)}), h(\mathbf{y}^{(i)}) \right) - \boldsymbol{\mu} \right) \left(g \left(f(\mathbf{x}^{(i)}), h(\mathbf{y}^{(i)}) \right) - \boldsymbol{\mu} \right)^T, \quad (5)$$

$$\hat{\boldsymbol{\Sigma}} = \frac{1}{M-1} \sum_{i=0}^M \left(g \left(f(\hat{\mathbf{x}}^{(i)}), h(\hat{\mathbf{y}}^{(i)}) \right) - \hat{\boldsymbol{\mu}} \right) \left(g \left(f(\hat{\mathbf{x}}^{(i)}), h(\hat{\mathbf{y}}^{(i)}) \right) - \hat{\boldsymbol{\mu}} \right)^T. \quad (6)$$

Note that by computing the FD over the joint image-conditioning distribution, we are able to simultaneously assess image quality, conditional consistency, and intra-conditioning diversity, all of which are important factors in evaluating the quality of conditional image generation models.

FJD uses the same image embedding function as the FID score, namely a pre-trained Inception v3 model [39]. The choice of h and g are discussed in the remainder of this section.

Conditioning embedding function: h . The purpose of the embedding function h is to reduce the dimensionality and extract a useful feature representation of the conditioning. As such, the choice of h will vary depending on the type of conditioning. As the majority of the conditioning used in our experiments contains spatial information, we use a pre-trained Inception v3 model³ to embed all class, bounding box, and mask conditioning into a single unified space for our experiments. Class labels are tiled spatially so that they have the same height and width as the images.

To match the required dimensionality of the image embedding with that of the conditioning, we apply a fixed linear random projection r to the conditioning tensor $\mathbf{y} \in \mathbb{R}^{H,W,C}$, where H , W and C represent tensor height, width and number of channels, respectively. As a result, we obtain an embedded conditioning matching the dimensionality of the image space $r(\mathbf{y}) \in \mathbb{R}^{H,W,3}$. An example of the conditioning after random projection can be found in Figure 1. After projection, we feed $r(\mathbf{y})$ through an Inception v3 network to extract a 2048-dimensional embedding $f(r(\mathbf{y}))$ from the final pooling layer. Finally, we multiply the conditioning embedding by a scaling factor α , where α allows us to control for the relative importance of f versus h . Note that if the magnitude of the image embedding is much greater than that of the conditioning embedding, then a generative model that produces good quality images without regard for the conditioning may score the same as a model that does properly respect conditioning, reducing the effectiveness of the metric.

We do not scale the image embedding so that it can act as a reference magnitude comparable with FID. As a recommendation we suggest setting α to be equal to the ratio between the average L_2 norm of the image embedding and the conditioning embedding. We note that α should be calculated on data from the reference distribution (real data distribution), and then applied to all conditioning embeddings thereafter. Thus, $h(\mathbf{y}) = \alpha f(r(\mathbf{y}))$.

Merging function: g . We consider and evaluate four different merging strategies: (1) concatenation $g(f(\mathbf{x}), h(\mathbf{y})) = [f(\mathbf{x}), h(\mathbf{y})]$, where $[\]$ represents the vector concatenation operation; (2) summation $g(f(\mathbf{x}), h(\mathbf{y})) = f(\mathbf{x}) + h(\mathbf{y})$; (3) element-wise multiplication $g(f(\mathbf{x}), h(\mathbf{y})) = f(\mathbf{x}) \odot h(\mathbf{y})$; and (4) random projection $g(f(\mathbf{x}), h(\mathbf{y})) = r'([f(\mathbf{x}), h(\mathbf{y})])$, where r' is a linear random projection. Although all discussed merging strategies are suitable to represent joint image-conditioning embeddings, we recommend using concatenation due to it providing the best correlation with conditional consistency in our experiments. We refer the reader to the supplementary material for a detailed ablation study.

³We use the PyTorch pre-trained Inception v3 in our experiments.

5 Evaluation of Fréchet Joint Distance

In this section, we start by introducing the datasets used in our analysis. we then demonstrate that FJD captures the three desiderata of conditional image generation, namely image quality, conditional consistency and intra-conditioning diversity.

5.1 Datasets

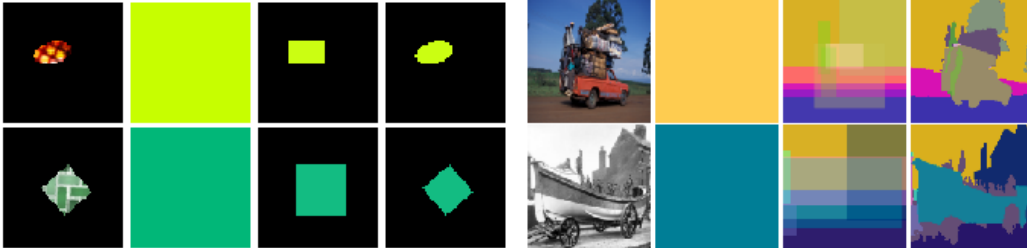


Figure 1: Image, class, bounding box, and mask samples: dSprite-textures (left), COCO-Stuff (right). **dSprite-textures.** The dSprite dataset [23] is a synthetic dataset where each image depicts a simple 2D shape on a black background. Each image can be fully described by a set of factors, including shape, scale, rotation, x position, and y position. We augment the dSprite dataset to create *dSprite-textures* by adding seven texture patterns for each sample. Additionally, we include class labels indicating shape, as well as bounding boxes and mask labels for each sample (see Figure 1 (left)). In total, the dataset contains 5,160,960 unique images. This synthetic dataset allows us to exactly control our sample distribution and, thereby, simulate a generator with desired image-conditioning inconsistencies.

COCO-Stuff. The COCO-Stuff dataset [7] consists of 164,000 natural images with pixel-level annotations, including 80 “thing” classes and 91 “stuff” classes. Following [17], we select only images containing between 3 and 8 objects, and also ignore any objects that occupy less than 2% of the total image area. After filtering the dataset we are left with 74,121 training images and 3,074 validation images. Similar to our dSprite-textures dataset, COCO-Stuff provides image-level class labels, as well as bounding boxes and mask annotations. Examples of images together with available annotations are depicted on Figure 1 (right).

5.2 Image Quality

In this subsection, we aim to test the sensitivity of FJD to image quality perturbations. To do so, we use either a random draw of 10k dSprite-textures samples, or the entire COCO-Stuff training set. By duplicating each set of samples, we build a *reference* dataset and a *generated* dataset. Then, we simulate a generative model that produces low quality images by adding Gaussian noise drawn from $\mathcal{N}(0, \sigma)$ to the generated dataset images and then clipping to the data range, where $\sigma \in [0, 0.25]$ and pixel values are normalized to the range $[0, 1]$. We repeat this experiment for both dSprite-textures and COCO-Stuff datasets and all three types of conditioning: class, bounding box, and mask.

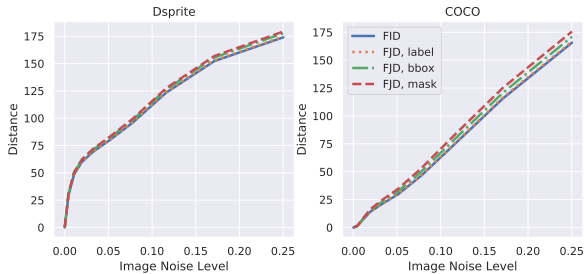


Figure 2: **Image quality:** Comparison between FID and FJD for class, bounding box, and mask conditioning under varying noise levels added to images.

Results are shown in Figure 2, where we plot both FID and FJD scores as a function of the added Gaussian noise (σ is indicated on the x -axis as Image Noise Level). We find that, in all cases, FJD tracks FID very closely, indicating that it successfully captures image quality. Interestingly, we note that FJD increases slightly compared to FID as image quality decreases, likely due to a decrease in perceived conditional consistency.

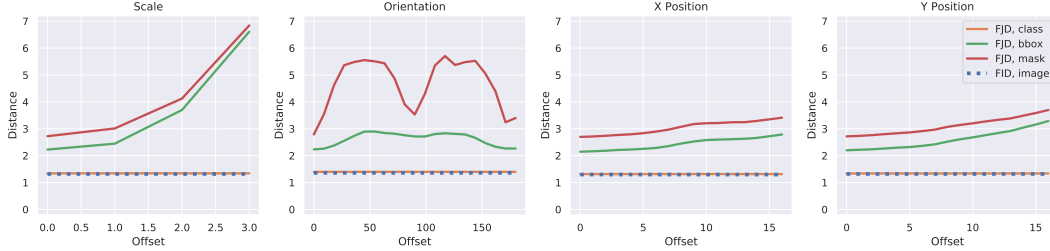


Figure 3: **Conditional consistency:** Change in FJD with respect to offset on Dsprite-textures dataset for class, bounding box and mask conditionings.

5.3 Conditional Consistency

In this subsection, we aim to highlight the sensitivity of FJD to conditional consistency. In particular, we target specific types of inconsistencies, such as incorrect scale, orientation, or position. For these experiments, we use only the dSprite-textures dataset, where we can control the degree to which conditional consistency is violated. We draw two sets of 10k samples from the dSprite-textures dataset: one to represent a reference dataset, and another to represent a generated dataset. For 30% of the generated dataset samples we swap conditionings of pairs of samples that are identical in all but one of the attributes (scale, orientation, x position or y position). For example, if one generated sample has attribute x position 4 and a second generated sample has attribute x position 7, swapping their conditionings leads to generated samples that are offset by 3 pixels w.r.t. their ground truth x position. Swapping conditionings in this manner allows us to control for specific attributes' conditional consistency, while keeping the image and conditioning marginal distributions unchanged. As a result, all changes in FJD can be attributed solely to conditional inconsistencies.

Figure 3 depicts the results of this experiment for four different types of alterations: scale, orientation, and x and y positions. We observe that the FID between image distributions (blue dashed line) remains constant even as the conditional inconsistencies increase. For class conditioning (solid orange line), FJD remains constant, as changes to scale, orientation, and position are independent of the object class. Bounding box and mask conditionings, as they contain spatial information, produce variations in FJD that are proportional to the offset. Interestingly, for the orientation offsets, FJD with mask conditioning fluctuates rather than increasing monotonically. This behaviour is due to the orientation-masks partially re-aligning around 90° and 180° . Each of these cases emphasize the effective sensitivity of FJD w.r.t. conditional consistency.

5.4 Intra-conditioning Diversity

In this subsection, we aim to test the sensitivity of FJD to intra-conditioning diversity. To do so, we experiment with the dSprite-textures dataset, as it allows us to simulate intra-conditioning diversity.⁴ We create our reference dataset by randomly drawing 10k samples using only three textures. Subsequently, we create less diverse generated datasets by duplicating the reference dataset and then reducing the texture variability by increasing the proportion of points that are assigned to a unique texture type. Moreover, we associate the choice of unique textures with different subsets of the dataset, partitioned by attributes (shapes, scale, orientation, position); this allows us to study the effect of conditioning type on the metric's sensitivity to changes in diversity. Finally, we make these modifications in such a way that the marginal distribution of textures over the entire dataset is still roughly uniform.

The results of these experiments are shown in Figure 4, which plots the increase in FID and FJD, for different types of conditioning, as the diversity of textures decreases. Here, diversity of 1 means that all combinations of textures/attributes are possible, while diversity of 0 means that each texture is associated to a unique subset of attribute values. Not surprisingly, since a change in the joint distribution of attributes and textures also implies a change to the image marginal distribution, we observe that FID increases with reduced diversity. However, the increase in FJD is larger than the increase in FID, suggesting that FJD is more sensitive to changes in intra-conditioning diversity

⁴Note that for real datasets, intra-conditioning diversity is most often reduced as the strength of conditioning increases (e.g. mask conditionings usually present a single image instantiation, presenting no diversity).

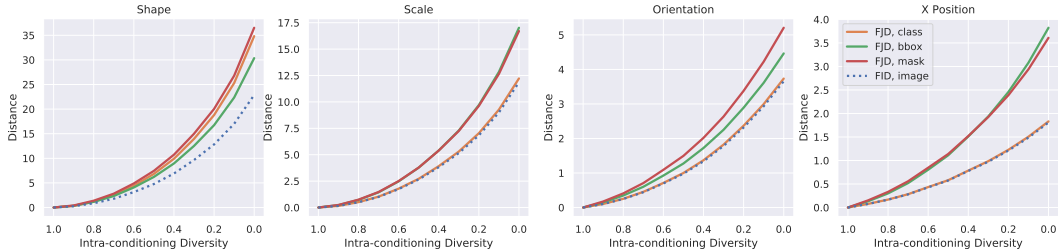


Figure 4: **Intra-conditioning diversity:** FJD and FID as intra-conditioning diversity decreases.

Table 1: FJD / FID results averaged over 5 runs on COCO-stuff validation set with class, bounding box (bbox) and mask conditionings for image resolutions 64×64 and 128×128 .

	class conditioning		bbox conditioning		mask conditioning	
	FJD ↓	FID ↓	FJD ↓	FID ↓	FJD ↓	FID ↓
64	31.7 ± 0.2	30.5 ± 0.2	43.2 ± 0.7	30.8 ± 0.7	52.8 ± 1.1	28.0 ± 1.0
128	42.7 ± 1.8	41.6 ± 1.8	54.5 ± 1.1	43.1 ± 1.1	62.1 ± 1.3	37.7 ± 1.2

than FID. It is interesting to note that FJD only increases over FID when the conditioning contains information related to the attribute that is losing internal diversity. For example, as the textural diversity within the shape attribute is reduced, FJD with all conditioning types increases over FID, as they all contain class information about the shape. However, in cases when such information is not present in the conditioning, such as in the case of scale, orientation, or position, FJD of class conditioning is similar in magnitude to FID.

6 An analysis of conditioning strengths

In this section, we aim to analyze how different conditioning strengths (class, bounding box, and mask) may influence image quality. To this end, we train three generative models, one for each conditioning type, on COCO-Stuff. Two image resolutions are considered: 64×64 and 128×128 . We adopt a BigGAN-style model [6], but modify the design such that a single fixed architecture can be trained with any of the three conditioning types. We do not fix the architecture across image resolutions: the 128 architecture has more capacity than the 64 one. Architecture details are provided in the supplementary material. We train each model 5 times, with different random seeds, and report mean and standard deviation of both FID and FJD in Table 1. As shown in the table, as we increase the conditioning strength (from class conditioning to mask conditioning), we notice a substantial increase in FJD score. We argue this is due to the information content present in each conditioning type. On the one hand, stronger conditionings (masks) present more information content, which in turn is easier to violate. On the other hand, weaker conditionings capture less information content and, hence, become easier to satisfy. When it comes to FID, we observe that the model with the strongest conditioning (mask-conditioned model) achieves the best results (lowest FID). We argue that stronger conditionings limit the degrees of freedom of the generation, and hence should be able to provide more plausible-looking images. Samples of conditional generations from all models are available in the supplementary material.

Table 2: Comparison of class-conditioned models on ImageNet validation set (resolution 128×128).

	FJD ↓	FID ↓	Acc. ↑
SN-GAN (concat) [25]	38.3	37.3	18.1
SN-GAN (proj) [25]	26.1	25.5	35.5
BigGAN [6]	10.2	9.9	62.3

7 Comparison of existing conditional generation models

In this section, we seek to evaluate existing cGAN-based models in terms of FJD, and to contrast these results to the ones provided by FID and standard conditional consistency metrics. In particular, we focus on testing class-conditioned and image-conditioned image generation as they deal with different conditioning strength and have been the focus of numerous works.

Table 3: Comparison of image-conditioned models. Results averaged over 50 runs (validation).

Dataset	Facades			Maps		
	FJD ↓	FID ↓	SSIM ↑	FJD ↓	FID ↓	SSIM ↑
Pix2pix [16]	171.2 ± 0.0	115.7 ± 0.0	23.0 ± 6.7	352.6 ± 0.0	230.4 ± 0.0	14.8 ± 8.3
BicycleGAN [58]	152.2 ± 2.3	93.8 ± 2.2	20.6 ± 6.8	275.4 ± 1.0	152.7 ± 1.0	14.8 ± 7.2
MSGAN [22]	154.3 ± 2.3	97.5 ± 2.3	17.7 ± 6.6	273.4 ± 2.0	152.0 ± 2.0	10.9 ± 7.5
	Edges2Shoes			Edges2Handbags		
Pix2pix [16]	164.9 ± 0.0	121.9 ± 0.0	64.3 ± 14.0	148.6 ± 0.0	82.7 ± 0.0	61.4 ± 13.7
BicycleGAN [58]	88.2 ± 1.2	47.6 ± 1.1	69.1 ± 9.8	142.6 ± 1.3	76.6 ± 1.2	58.6 ± 13.9
MUNIT [15]	97.1 ± 1.3	55.5 ± 1.3	67.7 ± 10.0	147.8 ± 1.4	79.5 ± 1.3	54.2 ± 13.9

Class-conditioned cGANs. Table 2 presents FJD, FID, and classification accuracy results for three state-of-the-art class-conditioned models trained on ImageNet⁵. Accuracy is computed as the Inception v3 accuracy of each model’s generated samples, using their conditioning as classification ground truth, and is presented as conditional consistency metric. Results are reported for an image resolution of 128×128 on the validation set. We find that FJD follows the same trend as FID for class-conditioned models, preserving their ranking and highlighting the FJD’s ability to capture image quality. However, it is worth noting that all models exhibit a slightly higher FJD as compared to FID, emphasizing each model’s potential conditional inconsistencies. When comparing FJD to accuracy, we observe that FJD is also coherent with the conditional consistency metric (higher FJD values correlate with lower accuracies), confirming its ability to properly assess conditional consistency. Overall, BigGAN seems to demonstrate the best trade-off between image quality and conditional consistency, followed by SN-GAN (projection), while SN-GAN (concatenation) exhibits the weakest performance among compared models.

Image-conditioned cGANs. Table 3 provides the FJD, FID, and SSIM scores for state-of-the-art models on four different image-to-image datasets: Facades [31], Maps [16], Edges2Shoes and Edges2Handbag [56].⁶ We consider the validation set associated with each of the datasets and obtain one sample per conditioning for each model. We repeat this experiment 50 times and report the mean and standard deviation for the three metrics. This experiment highlights the difficulty of ranking models when using two independent metrics for image quality and conditional consistency. In all datasets except Edges2Shoes, ranking the models in terms of average FID leads to a different outcome than ranking them based on their average SSIM. Although FJD follows a similar ranking to FID, we have seen in Section 5 that the metric is sensitive to image quality, conditional inconsistencies and intra-conditioning diversity, simultaneously. When considering Facades and Edges2Handbags datasets, we observe that pix2pix achieves better conditional consistency as measured by SSIM. However, its FJD is higher than that of BicycleGAN, suggesting that it may be penalized for lower image quality or lack of intra-conditioning diversity. Similarly, in the Maps dataset, MSGAN shows better average FID, whereas BicycleGAN achieves better conditional consistency. When it comes to comparing their FJD values, we note that, on average, MSGAN is better (although not significantly).

8 Conclusions

In this paper we introduce Fréchet Joint Distance (FJD), which is able to assess image quality, conditional consistency, and intra-conditioning diversity within a single metric. We compared FJD to FID on the synthetic dSprite-textures dataset and on the large-scale COCO-Stuff dataset, validating its ability to capture the three properties of interest across different types of conditioning, and highlighting its potential to be adopted as unified cGAN benchmarking metric.

Looking forward, FJD could serve as valuable metric to ground future research, as it has the potential to help elucidate the most promising contributions within the scope of conditional generation. A possible future direction would be to adapt the metric to other types of conditioning such as text,

⁵Pre-trained models: BigGAN from <https://github.com/ajbrock/BigGAN-PyTorch> and SN-GAN https://github.com/pfnet-research/sngan_projection

⁶Pre-trained models: pix2pix from <https://github.com/junyanz/pytorch-CycleGAN-and-pix2pix>, BicycleGAN from <https://github.com/junyanz/BicycleGAN>, MSGAN from <https://github.com/HelenMao/MSGAN/> and MUNIT from <https://github.com/nv1labs/MUNIT>.

graphs or dialogue. Finally, with this metric, we have reinforced a known limitation of current datasets, namely that in the case of strong conditionings, datasets only contain a single instantiation per conditioning that we hope to see addressed in the near future.

Acknowledgements The authors would like to thank Nicolas Ballas, Lluís Castrejon, Mohamed Ishmael Belghazi, Nissan Pow, Mido Assran, Anton Bakhtin, and Vinakayk Tantia for useful and entertaining discussions.

References

- [1] Amjad Almahairi, Sai Rajeshwar, Alessandro Sordani, Philip Bachman, and Aaron Courville. Augmented CycleGAN: Learning many-to-many mappings from unpaired data. In Jennifer Dy and Andreas Krause, editors, *Proceedings of the 35th International Conference on Machine Learning*, volume 80 of *Proceedings of Machine Learning Research*, pages 195–204, Stockholmsmässan, Stockholm Sweden, 10–15 Jul 2018. PMLR.
- [2] Martin Arjovsky, Soumith Chintala, and Léon Bottou. Wasserstein generative adversarial networks. In Doina Precup and Yee Whye Teh, editors, *Proceedings of the 34th International Conference on Machine Learning*, volume 70 of *Proceedings of Machine Learning Research*, pages 214–223, International Convention Centre, Sydney, Australia, 06–11 Aug 2017. PMLR.
- [3] Satyanjeev Banerjee and Alon Lavie. Meteor: An automatic metric for mt evaluation with improved correlation with human judgments. In *Proceedings of the acl workshop on intrinsic and extrinsic evaluation measures for machine translation and/or summarization*, pages 65–72, 2005.
- [4] Mikołaj Bińkowski, Dougal J. Sutherland, Michael Arbel, and Arthur Gretton. Demystifying MMD GANs. In *International Conference on Learning Representations*, 2018.
- [5] Ali Borji. Pros and cons of GAN evaluation measures. *CoRR*, abs/1802.03446, 2018.
- [6] Andrew Brock, Jeff Donahue, and Karen Simonyan. Large scale GAN training for high fidelity natural image synthesis. In *International Conference on Learning Representations*, 2019.
- [7] Holger Caesar, Jasper R. R. Uijlings, and Vittorio Ferrari. Coco-stuff: Thing and stuff classes in context. In *CVPR*, pages 1209–1218. IEEE Computer Society, 2018.
- [8] Alaaeldin El-Nouby, Shikhar Sharma, Hannes Schulz, R. Devon Hjelm, Layla El Asri, Samira Ebrahimi Kahou, Yoshua Bengio, and Graham W. Taylor. Tell, draw, and repeat: Generating and modifying images based on continual linguistic instruction. *CoRR*, abs/1811.09845, 2019.
- [9] Ian Goodfellow, Jean Pouget-Abadie, Mehdi Mirza, Bing Xu, David Warde-Farley, Sherjil Ozair, Aaron Courville, and Yoshua Bengio. Generative adversarial nets. In Z. Ghahramani, M. Welling, C. Cortes, N. D. Lawrence, and K. Q. Weinberger, editors, *Advances in Neural Information Processing Systems 27*, pages 2672–2680. Curran Associates, Inc., 2014.
- [10] Arthur Gretton, Karsten M. Borgwardt, Malte J. Rasch, Bernhard Schölkopf, and Alexander Smola. A kernel two-sample test. *J. Mach. Learn. Res.*, 13(1):723–773, March 2012.
- [11] Swaminathan Gurumurthy, Ravi Kiran Sarvadevabhatla, and R. Venkatesh Babu. Deligan: Generative adversarial networks for diverse and limited data. In *Computer Vision and Pattern Recognition*, pages 4941–4949. IEEE Computer Society, 2017.
- [12] Martin Heusel, Hubert Ramsauer, Thomas Unterthiner, Bernhard Nessler, and Sepp Hochreiter. Gans trained by a two time-scale update rule converge to a local nash equilibrium. In I. Guyon, U. V. Luxburg, S. Bengio, H. Wallach, R. Fergus, S. Vishwanathan, and R. Garnett, editors, *Advances in Neural Information Processing Systems 30*, pages 6626–6637. Curran Associates, Inc., 2017.
- [13] Tobias Hinz, Stefan Heinrich, and Stefan Wermter. Generating multiple objects at spatially distinct locations. In *International Conference on Learning Representations*, 2019.
- [14] Seunghoon Hong, Dingdong Yang, Jongwook Choi, and Honglak Lee. Inferring semantic layout for hierarchical text-to-image synthesis. In *Computer Vision and Pattern Recognition*, pages 7986–7994. IEEE Computer Society, 2018.
- [15] Xun Huang, Ming-Yu Liu, Serge Belongie, and Jan Kautz. Multimodal unsupervised image-to-image translation. In *ECCV*, 2018.
- [16] Phillip Isola, Jun-Yan Zhu, Tinghui Zhou, and Alexei A Efros. Image-to-image translation with conditional adversarial networks. *Computer Vision and Pattern Recognition (CVPR)*, 2017.
- [17] Justin Johnson, Agrim Gupta, and Li Fei-Fei. Image generation from scene graphs. In *CVPR*, pages 1219–1228. IEEE Computer Society, 2018.
- [18] Felix Juefei-Xu, Vishnu Naresh Boddeti, and Marios Savvides. Gang of gans: Generative adversarial networks with maximum margin ranking. *CoRR*, abs/1704.04865, 2017.

- [19] Tero Karras, Timo Aila, Samuli Laine, and Jaakko Lehtinen. Progressive growing of GANs for improved quality, stability, and variation. In *International Conference on Learning Representations*, 2018.
- [20] Diederik P. Kingma and Max Welling. Auto-encoding variational bayes. In *ICLR*, 2014.
- [21] E. L. Lehmann and Joseph P. Romano. *Testing statistical hypotheses*. Springer Texts in Statistics. Springer, third edition, 2005.
- [22] Qi Mao, Hsin-Ying Lee, Hung-Yu Tseng, Siwei Ma, and Ming-Hsuan Yang. Mode seeking generative adversarial networks for diverse image synthesis. In *IEEE Conference on Computer Vision and Pattern Recognition*, 2019.
- [23] Loic Matthey, Irina Higgins, Demis Hassabis, and Alexander Lerchner. dsprites: Disentanglement testing sprites dataset. <https://github.com/deepmind/dsprites-dataset/>, 2017.
- [24] Mehdi Mirza and Simon Osindero. Conditional generative adversarial nets. *CoRR*, abs/1411.1784, 2014.
- [25] Takeru Miyato, Toshiki Kataoka, Masanori Koyama, and Yuichi Yoshida. Spectral normalization for generative adversarial networks. In *International Conference on Learning Representations*, 2018.
- [26] Takeru Miyato and Masanori Koyama. cGANs with projection discriminator. In *International Conference on Learning Representations*, 2018.
- [27] Augustus Odena, Christopher Olah, and Jonathon Shlens. Conditional image synthesis with auxiliary classifier GANs. In *Proceedings of the 34th International Conference on Machine Learning - Volume 70, ICML'17*, pages 2642–2651. JMLR.org, 2017.
- [28] Kishore Papineni, Salim Roukos, Todd Ward, and Wei-Jing Zhu. Bleu: a method for automatic evaluation of machine translation. In *Proceedings of the 40th annual meeting on association for computational linguistics*, pages 311–318. Association for Computational Linguistics, 2002.
- [29] Taesung Park, Ming-Yu Liu, Ting-Chun Wang, and Jun-Yan Zhu. Semantic image synthesis with spatially-adaptive normalization. In *Proceedings of the IEEE Conference on Computer Vision and Pattern Recognition*, 2019.
- [30] Alec Radford, Luke Metz, and Soumith Chintala. Unsupervised representation learning with deep convolutional generative adversarial networks. In *International Conference on Learning Representations*, 2016.
- [31] Radim Šára Radim Tyleček. Spatial pattern templates for recognition of objects with regular structure. In *Proc. GCPR*, Saarbrücken, Germany, 2013.
- [32] Scott Reed, Zeynep Akata, Xinchun Yan, Lajanugen Logeswaran, Bernt Schiele, and Honglak Lee. Generative adversarial text to image synthesis. In *Proceedings of the 33rd International Conference on Machine Learning - Volume 48, ICML'16*, pages 1060–1069. JMLR.org, 2016.
- [33] Tim Salimans, Ian Goodfellow, Wojciech Zaremba, Vicki Cheung, Alec Radford, Xi Chen, and Xi Chen. Improved techniques for training gans. In D. D. Lee, M. Sugiyama, U. V. Luxburg, I. Guyon, and R. Garnett, editors, *Advances in Neural Information Processing Systems 29*, pages 2234–2242. Curran Associates, Inc., 2016.
- [34] Amaia Salvador, Michal Drozdal, Xavier Giró i Nieto, and Adriana Romero. Inverse cooking: Recipe generation from food images. In *Computer Vision and Patter Recognition (CVPR)*. IEEE Computer Society, 2019.
- [35] Iulian Vlad Serban, Alessandro Sordoni, Ryan Lowe, Laurent Charlin, Joelle Pineau, Aaron C. Courville, and Yoshua Bengio. A hierarchical latent variable encoder-decoder model for generating dialogues. In *AAAI*, pages 3295–3301. AAAI Press, 2017.
- [36] Shikhar Sharma, Dendi Suhubdy, Vincent Michalski, Samira Ebrahimi Kahou, and Yoshua Bengio. Chatpainter: Improving text to image generation using dialogue. *CoRR*, abs/1802.08216, 2018.
- [37] Jake Snell, Karl Ridgeway, Renjie Liao, Brett D. Roads, Michael C. Mozer, and Richard S. Zemel. Learning to generate images with perceptual similarity metrics. In *2017 IEEE International Conference on Image Processing, ICIP 2017, Beijing, China, September 17-20, 2017*, pages 4277–4281, 2017.
- [38] Sandeep Subramanian, Sai Rajeswar Mudumba, Alessandro Sordoni, Adam Trischler, Aaron C Courville, and Chris Pal. Towards text generation with adversarially learned neural outlines. In S. Bengio, H. Wallach, H. Larochelle, K. Grauman, N. Cesa-Bianchi, and R. Garnett, editors, *Advances in Neural Information Processing Systems 31*, pages 7551–7563. Curran Associates, Inc., 2018.
- [39] Christian Szegedy, Vincent Vanhoucke, Sergey Ioffe, Jonathon Shlens, and Zbigniew Wojna. Rethinking the inception architecture for computer vision. In *CVPR*, pages 2818–2826. IEEE Computer Society, 2016.
- [40] Qiuyuan Huang Han Zhang Zhe Gan Xiaolei Huang Xiaodong He Tao Xu, Pengchuan Zhang. Attngan: Fine-grained text to image generation with attentional generative adversarial networks. 2018.

- [41] Lucas Theis, Aäron van den Oord, and Matthias Bethge. A note on the evaluation of generative models. In *International Conference on Learning Representations*, 2016.
- [42] Aaron van den Oord, Nal Kalchbrenner, Lasse Espeholt, koray kavukcuoglu, Oriol Vinyals, and Alex Graves. Conditional image generation with pixelcnn decoders. In D. D. Lee, M. Sugiyama, U. V. Luxburg, I. Guyon, and R. Garnett, editors, *Advances in Neural Information Processing Systems 29*, pages 4790–4798. Curran Associates, Inc., 2016.
- [43] Aäron Van Den Oord, Nal Kalchbrenner, and Koray Kavukcuoglu. Pixel recurrent neural networks. In *Proceedings of the 33rd International Conference on International Conference on Machine Learning - Volume 48*, ICML’16, pages 1747–1756. JMLR.org, 2016.
- [44] Aäron van den Oord, Sander Dieleman, Heiga Zen, Karen Simonyan, Oriol Vinyals, Alexander Graves, Nal Kalchbrenner, Andrew Senior, and Koray Kavukcuoglu. Wavenet: A generative model for raw audio. In *Arxiv*, 2016.
- [45] Ramakrishna Vedantam, C Lawrence Zitnick, and Devi Parikh. Cider: Consensus-based image description evaluation. In *Proceedings of the IEEE conference on computer vision and pattern recognition*, pages 4566–4575, 2015.
- [46] Carl Vondrick, Hamed Pirsiavash, and Antonio Torralba. Generating videos with scene dynamics. In D. D. Lee, M. Sugiyama, U. V. Luxburg, I. Guyon, and R. Garnett, editors, *Advances in Neural Information Processing Systems 29*, pages 613–621. Curran Associates, Inc., 2016.
- [47] Ting-Chun Wang, Ming-Yu Liu, Jun-Yan Zhu, Andrew Tao, Jan Kautz, and Bryan Catanzaro. High-resolution image synthesis and semantic manipulation with conditional gans. In *Proceedings of the IEEE Conference on Computer Vision and Pattern Recognition*, 2018.
- [48] Zhou Wang, Alan C. Bovik, Hamid R. Sheikh, and Eero P. Simoncelli. Image quality assessment: From error visibility to structural similarity. *IEEE TRANSACTIONS ON IMAGE PROCESSING*, 13(4):600–612, 2004.
- [49] Sitao Xiang and Hao Li. On the effects of batch and weight normalization in generative adversarial networks. *arXiv preprint arXiv:1704.03971*, 2017.
- [50] Jianwei Yang, Anitha Kannan, Dhruv Batra, and Devi Parikh. LR-GAN: layered recursive generative adversarial networks for image generation. In *International Conference on Learning Representations*. OpenReview.net, 2017.
- [51] Han Zhang, Tao Xu, Hongsheng Li, Shaoting Zhang, Xiaogang Wang, Xiaolei Huang, and Dimitris Metaxas. Stackgan: Text to photo-realistic image synthesis with stacked generative adversarial networks. In *ICCV*, 2017.
- [52] Han Zhang, Tao Xu, Hongsheng Li, Shaoting Zhang, Xiaogang Wang, Xiaolei Huang, and Dimitris N. Metaxas. Stackgan++: Realistic image synthesis with stacked generative adversarial networks. *IEEE Transactions on Pattern Analysis and Machine Intelligence*, July 2018.
- [53] Richard Zhang, Phillip Isola, Alexei A Efros, Eli Shechtman, and Oliver Wang. The unreasonable effectiveness of deep features as a perceptual metric. In *CVPR*, 2018.
- [54] Bo Zhao, Lili Meng, Weidong Yin, and Leonid Sigal. Image generation from layout. In *Computer Vision and Pattern Recognition*. IEEE Computer Society, 2019.
- [55] Zhiming Zhou, Han Cai, Shu Rong, Yuxuan Song, Kan Ren, Weinan Zhang, Jun Wang, and Yong Yu. Activation maximization generative adversarial nets. In *International Conference on Learning Representations*, 2018.
- [56] Jun-Yan Zhu, Philipp Krähenbühl, Eli Shechtman, and Alexei A. Efros. Generative visual manipulation on the natural image manifold. In *Computer Vision - ECCV 2016 - 14th European Conference, Amsterdam, The Netherlands, October 11-14, 2016, Proceedings, Part V*, pages 597–613, 2016.
- [57] Jun-Yan Zhu, Taesung Park, Phillip Isola, and Alexei A Efros. Unpaired image-to-image translation using cycle-consistent adversarial networks. In *Computer Vision (ICCV), 2017 IEEE International Conference on*, 2017.
- [58] Jun-Yan Zhu, Richard Zhang, Deepak Pathak, Trevor Darrell, Alexei A Efros, Oliver Wang, and Eli Shechtman. Toward multimodal image-to-image translation. In *Advances in Neural Information Processing Systems*, 2017.

Supplementary Material: On the Evaluation of Conditional GANs

A Illustration of FID and FJD on two dimensional Gaussian data

In this section, we illustrate the claim made in Section 1 that FID cannot capture intra-conditioning diversity when the joint distribution of two variables changes but the marginal distribution of one of them is not altered.

Consider two multivariate Gaussian distributions, $(X_1, Y_1) \sim \mathcal{N}(\mathbf{0}, \Sigma_1)$ and $(X_2, Y_2) \sim \mathcal{N}(\mathbf{0}, \Sigma_2)$, where

$$\Sigma_1 = \begin{bmatrix} 4 & 2 \\ 2 & 2 \end{bmatrix} \quad \Sigma_2 = \begin{bmatrix} 2.1 & 2 \\ 2 & 2 \end{bmatrix}.$$

Figure 5 (left) shows 10,000 samples drawn from each of these distributions, labeled as Dist1 and Dist2, respectively. While the joint distributions of $f_{X_1, Y_1}(X_1, Y_1)$ and $f_{X_2, Y_2}(X_2, Y_2)$ are different from each other, the marginal distributions $f_{Y_1}(Y_1)$ and $f_{Y_2}(Y_2)$ are the same ($Y_1 \sim \mathcal{N}(0, 2)$ and $Y_2 \sim \mathcal{N}(0, 2)$). Figure 5 (center) shows the histograms of the two marginal distributions computed from 10,000 samples.

If we let X_i take the role of the embedding of the conditioning variables (e.g., class labels) and Y_i take the role of the embedding of the generated variables (i.e., images), then computing FID in this example would correspond to computing the FD between f_{Y_1} and f_{Y_2} , which is *zero*. On the other hand, computing FJD would correspond to the FD between f_{X_1, Y_1} and f_{X_2, Y_2} , which equals 0.678. But note that Dist1 and Dist2 have different degrees of intra-conditioning diversity, as illustrated by Figure 5 (right), where two histograms of $f_{Y_i|X_i \in (0.9, 1.1)}$ are displayed, showing marked differences to each other (similar plots can be constructed for other values of X_i). Therefore, this example illustrates a situation in which FID is unable to capture changes in intra-conditioning diversity, while FJD is able to do so.

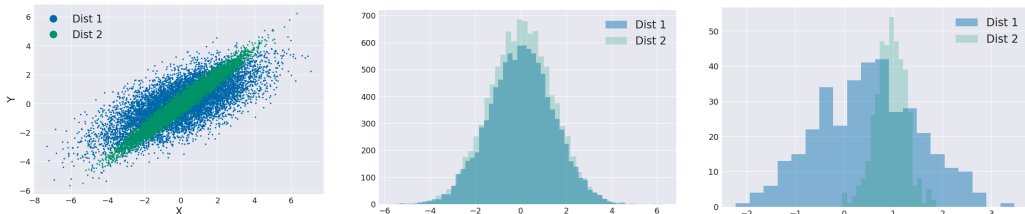


Figure 5: Left: samples from two multivariate Gaussian distributions. Center: Histograms of marginal distributions for Y variable. Right: Histogram of conditional distributions for Y conditioned on $X \in (0.9, 1.1)$.

B Evaluation of merging functions

To compare different merging functions, as described in Section 4, we evaluate how well the FJD of each joint distribution correlates to conditional consistency. To do so, we start by drawing 10k dSprite-textures samples, or the entire COCO-Stuff training set. By duplicating those samples, we build a *reference* dataset and a *generated* dataset. Then, we simulate a generative model that produces images that are inconsistent with the conditioning by randomly permuting a subset of the conditionings of the generated dataset, affecting the degree of conditional consistency. As a result, neither the image distribution nor the conditioning distribution of the generated dataset are changed, and the perturbation is only visible in the joint image-conditioning space. Thus, any change in FJD can be attributed solely to changes in conditional consistency, resulting in high correlation between the FJD score and the conditional consistency. Note that this experiment is repeated for three different types of conditioning: class-conditioning, bounding box-conditioning and mask-conditioning.

Figures 6 and 7 depict FJD as a function of conditional consistency for four merging functions (concatenation, summation, multiplication and projection) on dSprites-textures and COCO-Stuff datasets.

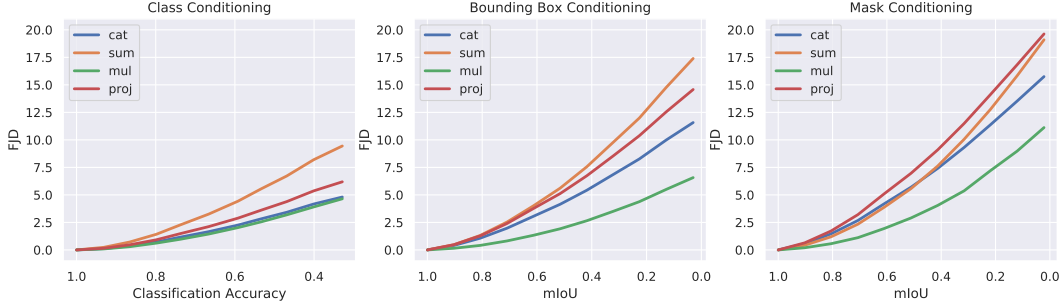


Figure 6: FJD merging functions on dSprite-textures as a function of conditional consistency.

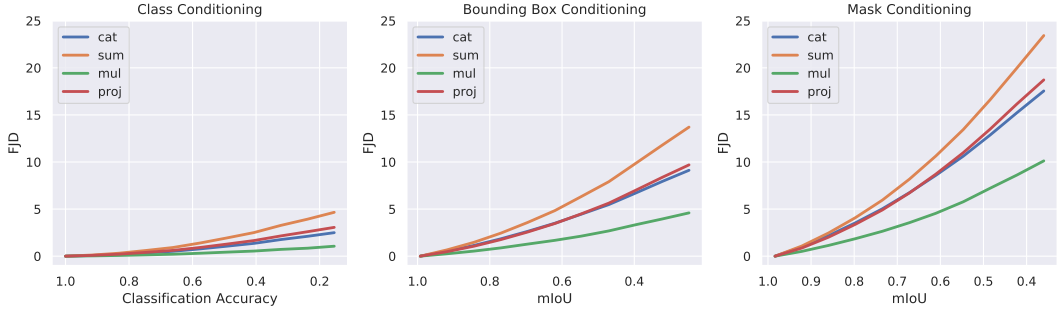


Figure 7: FJD merging functions on COCO-Stuff as a function of conditional consistency.

Following standard practice, we measure conditional consistency in terms of classification accuracy between the original class labels and the ones in the generated dataset, in the class-conditioned case. Analogously, we measure conditional consistency in terms of mIoU between the original bounding boxes/masks and the ones in the generated dataset. As shown in the figures, all considered merging functions are sensitive to conditional inconsistencies and they exhibit comparable behavior across both datasets. In particular, summation seems to consistently yield the highest FJD values across different conditioning types (except for the mask-conditioned case of dSprites-textures), followed by projection, concatenation and then multiplication. It is worth noting that, for the sake of comparison, the embedding dimensionality is preserved across merging functions.

Table 4 reports the correlation between FJD and conditional consistency for all merging functions and conditioning types on dSprites-textures and COCO-Stuff. As shown in the table, there is a strong negative correlation between FJD and conditional consistency for all candidate merging functions, highlighting that FJD effectively captures conditional consistency. Of the four strategies, simple embedding concatenation consistently demonstrated the best correlation (although by small margin) between FJD and conditional consistency across both conditioning types and datasets considered. As such, we recommend to use the concatenation as merging approach in FJD, and do so in our experiments.

Table 4: Correlation between FJD and conditional consistency for dSprite-textures and COCO-Stuff.

	dSprite-textures				COCO-stuff			
	Concat.	Sum.	Mult.	Proj.	Concat.	Sum.	Mult.	Proj.
accuracy	-0.986	-0.986	-0.980	-0.986	-0.978	-0.976	-0.974	-0.976
mIoU (bbox)	-0.988	-0.982	-0.975	-0.987	-0.991	-0.987	-0.989	-0.987
mIoU (mask)	-0.989	-0.974	-0.965	-0.987	-0.992	-0.986	-0.986	-0.988

C COCO-Stuff GAN Architecture Details

In order to modify BigGAN [6] to work with multiple types of conditioning we make two major changes. The first change occurs in the generator, where we replace the conditional batch normalization layers with SPADE [29]. This substitution allows the generator to receive spatial conditioning such as bounding boxes or masks. In the case of class conditioning with a spatially tiled class vector, SPADE behaves similarly to conditional batch normalization. The second change we make is in the discriminator. The original BigGAN implementation utilizes a single projection layer [26] in order to provide class conditional information to the discriminator. To extend this functionality to bounding box and mask conditioning, we add additional projection layers after each ResBlock in the discriminator. The input to each projection layer is a downsampled version of the conditioning that has been resized using nearest neighbour interpolation to match the spatial resolution of each layer. In this way we provide conditioning information at a range of resolutions, allowing the discriminator to use whichever is most useful for the type of conditioning it has received. Aside from these specified changes, models are trained with the same hyperparameters and training scheme as specified in [6].

D Samples of generated images

In this section, we present some 128×128 samples of conditional generation for the models covered in Section 6. In particular, Figures 8–10 show class, bounding box and mask conditioning samples, respectively. Each row displays a conditioning, followed by 4 different samples, and finally the real image corresponding to the conditioning. As shown in Figure 8, conditioning on classes leads to variable samples w.r.t. object positions, scales and textures. As we increase the conditioning strength, we reduce the freedom of the generation and hence, in Figure 9, we observe how the variability starts appearing in more subtle regions. Similarly, in Figure 10, taking different samples per conditioning only changes the textures. Although the degrees of variability decrease as the conditioning strength increases, we obtain sharper, better looking images.

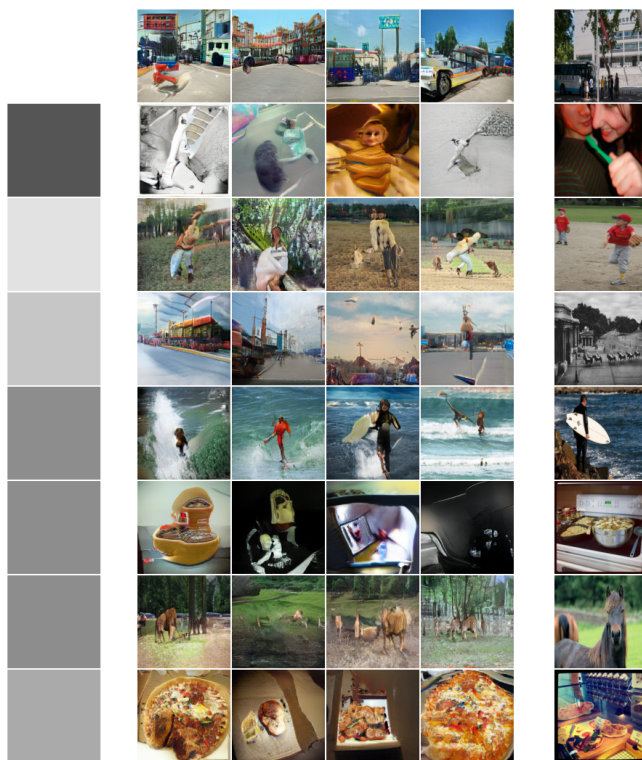


Figure 8: **Class-conditioning:** Conditioning, samples, and ground truth image for label conditioned GAN.

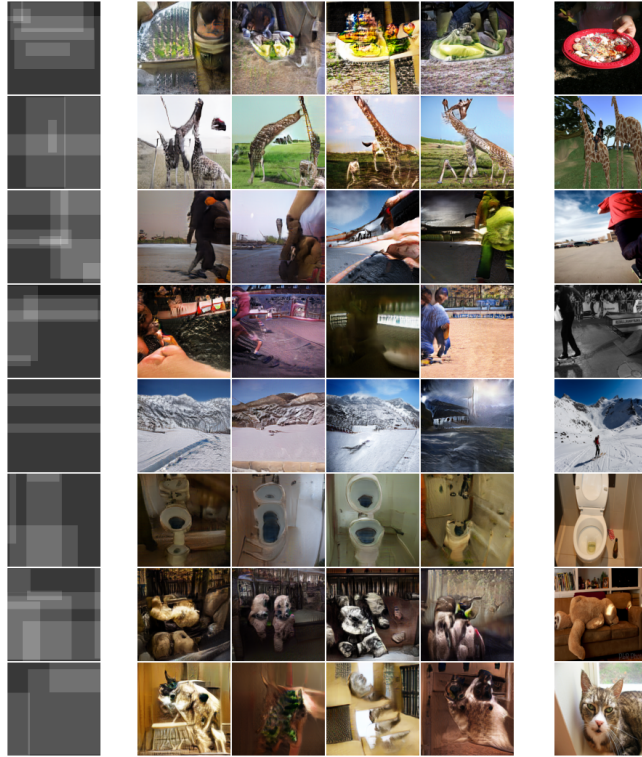


Figure 9: **Bounding box conditioning:** Conditioning, samples, and ground truth image for bounding box conditioned GAN.

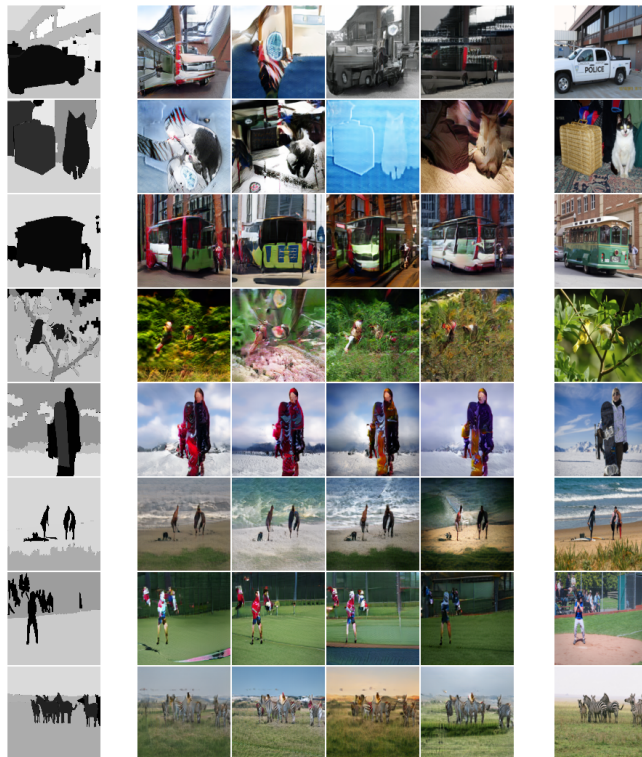


Figure 10: **Mask conditioning:** Conditioning, samples, and ground truth image for mask conditioned GAN.